

Electrically induced and tunable photonic band gap in submicron periodically poled lithium niobate

Z. Zhou · J. Shi · X. Chen

Received: 11 July 2008 / Revised version: 26 February 2009 / Published online: 27 June 2009
© Springer-Verlag 2009

Abstract We have theorized that a photonic band gap can be induced in a submicron periodically poled LiNbO₃ (SP-PPLN) with a uniform electrical field applied along the *Y* axis of the structure. The width of the band gap can be modulated by the intensity of the *Y*-directional electrical field. Moreover, for such a periodical structure with a duty cycle other than 0.5, the central location of the gap can be tuned by applying an additional electrical field along the *Z* axis of the sample.

PACS 42.70.Qs · 78.20.Jq

1 Introduction

Photonic crystals are a class of dielectric materials with artificially fabricated periodicity. With a proper design, they can exhibit photonic band gaps [1–3] as well as acquire potential applications in light-flow manipulations.

Nonlinear photonic crystals (NPCs) have been another attractive topic for their nonlinear coefficient χ_2 modulations [4]. The simplest type of NPC is the one-dimensional quasi-phase-matched material, first proposed by Armstrong et al. [5], in which the second order susceptibility undergoes a periodic change of sign. This type of structure can be fabricated by poling ferroelectric materials, such as LiNbO₃. The

formation of PPLN has been quite useful in quasi-phase-matching nonlinear interactions [6–8]. Moreover, the third-rank coefficients, such as electro-optic (EO) coefficients, are also periodically modulated and applicable in EO devices [9]. We have previously demonstrated a narrow-band solc-type filter on a single chip PPLN [10, 11] by EO modulations. The electric field would cause the optical axes of the crystal to rotate; thus, codirectional coupling is introduced between two orthogonally polarized states with the transmittances of filtering peak electrically controllable. The PPLN sample is fabricated by conventional photolithography techniques with pattern pitches of about tens of microns.

In recent years, electron-beam lithography and light-induced poling have developed with great interests and achieved pattern lines below 1 μm. It has been reported that in ferroelectrics domain engineering the scale of domain thickness of such ferroelectrics as KTiOPO₄ (KTP) isomorphs and LiNbO₃ has been improved to the level of several submicrons [12–16]. The technology of structuring submicrometer and nanometer scale domain patterns has driven us to study new optical properties as well as implement new optical devices, such as Bragg electro-optical reflectors.

As a result of previous research, one-dimensional periodical quasi-phase matching structure is well understood. Some promising results in fabricating one-dimensional aperiodic-engineered domain structures, fan-out domain structures, and two-dimensional nonlinear photonic crystal in lithium niobate have also been reported [17, 18]. In our discussion, we focus on the promising electrical methods to induce photonic band gaps in one-dimensional SP-PPLN. By applying an external electric field, contradirectional coupling between the two kinds of waves occurs in the submicron domain structure; therefore some wavelengths are totally reflected in which range the photonic band gap is

Z. Zhou · J. Shi (✉) · X. Chen
Department of Physics, The State Key Laboratory on Fiber-Optic Local Area Network and Advanced Optical Communication Systems, Shanghai Jiao Tong University, 800 Dongchuan Road, Shanghai 200240, China
e-mail: purewater@sjtu.edu.cn

X. Chen
e-mail: xfchen@sjtu.edu.cn

formed. The electrical method would be advantageous in tuning band gap properties, such as the gap width. Through the paper the properties of photonic band gaps are investigated by a traditional 4×4 matrix method. It is proved that both width and location of the band gap can be tuned by varying the electrical field. Some practical limitations are also discussed based on our theoretical models.

2 Basic theory

Figure 1 shows the schematic diagram of a Z-cut SPPLN photonic band gap structure. The arrows inside the SPPLN indicate spontaneous polarization directions. Λ is the period of SPPLN and κ is the proportional number defined by the length of the positive domain to the length of the period where $0 < \kappa < 1$.

It is well known that the transverse (Y -direction or Z -direction) electrical field would introduce electro-optic effects to the crystal. Since the magnitudes of electro-optic coefficients, such as γ_{51} , γ_{33} and γ_{13} , remain constant, but change signs in inverted domains, the electric-optic effect works differently in positive and negative domains according to their polarization orientations.

In the case of an electrical field applied along the Y axis of the sample, the deformation of the refractive index ellipsoid would cause the original principal axes at Y and Z directions to rotate to different Y' - and Z' -directions about the X axis [9]. As the principal axes in the positive and negative domains are periodically layered θ and $-\theta$, the filtering effect is demonstrated with two crossed polarizers placed at the two ends of the PPLN. In our applications each domain works as a zero-order half-wave plate at center filtering wavelengths [10, 11]. The rotation angle θ is defined by (1):

$$\theta \approx \frac{\gamma_{51} E_y}{(1/n_e)^2 - (1/n_o)^2} \quad (1)$$

where n_e and n_o are extraordinary and ordinary refractive indexes without an electrical field, γ_{51} is the electro-optic coefficient of LiNbO₃, and E_y is the applied field intensity along the Y axis.

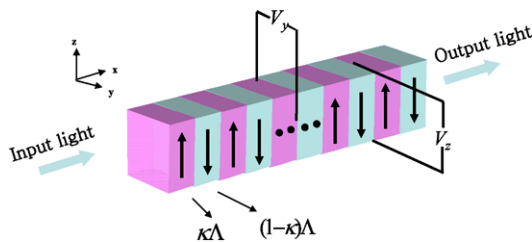


Fig. 1 Schematic diagram of the structure. X , Y , and Z represent the principal axes of the original index ellipsoid of LiNbO₃. The external electrical field is applied along the Y - and Z -directions

While the electrical field is along the Z axis, the principal axes remain unchanged in direction but vary in magnitude. The new refractive index in the positive and negative domains is defined by (2):

$$\begin{cases} n_e^\pm = n_e \mp \frac{1}{2} n_e^3 \cdot \gamma_{33} \cdot E_z, \\ n_o^\pm = n_o \mp \frac{1}{2} n_o^3 \cdot \gamma_{13} \cdot E_z \end{cases} \quad (2)$$

where γ_{33} and γ_{13} are its electro-optic coefficients and E_z is the applied electrical field along the Z axis. The subscripts + and - indicate positive and negative domains, respectively.

In our proposed periodical structure, while the domain length decreases down to a submicron which is comparable to the wavelength of incidence, contradirectional coupling between two orthogonally polarized modes would induce the forbidden band gaps occurrence in such media.

When the Y -directional electrical field E_y is applied alone, the refractive index remains constant in positive and negative domains, the Bragg reflection between two orthogonally polarized modes will occur when the following equation is satisfied [19]:

$$(k_1 + k_2) \cdot \kappa \Lambda + (k_1 + k_2)(1 - \kappa) \Lambda - 2m\pi = (k_1 + k_2) \Lambda - 2m\pi = 0, \quad m = 1, 2, 3 \dots \quad (3)$$

where k_1 and k_2 are the wave vectors defined by $\frac{2\pi n_e}{\lambda}$ and $\frac{2\pi n_o}{\lambda}$. When the additional electrical field E_z is applied, the refractive index in the positive and negative domains is not the same according to (2), thus (3) will be changed to the following form:

$$(k_1^+ + k_2^+) \cdot \kappa + (k_1^- + k_2^-) \cdot (1 - \kappa) - \frac{2m\pi}{\Lambda} = 0, \quad m = 1, 2, 3 \dots \quad (4)$$

where k_1^\pm and k_2^\pm are the wave-vectors defined by $\frac{2\pi n_e^\pm}{\lambda}$ and $\frac{2\pi n_o^\pm}{\lambda}$. The scripts + and - indicate the positive domain and negative domain, respectively. The coupling coefficients of these two modes are determined by the electrically induced rotation angle and the duty cycle of the structure.

The propagation of electromagnetic waves can be generally studied by transfer matrix methods. The electromagnetic waves traveling in birefringent crystals are composed of four partial waves, therefore the traditional 4×4 matrix is used which takes consideration of multilayer reflections and describes fine spectra. The transfer matrix of a single domain is the product of two component matrices D and P . For simplicity, here we just give the general results of matrices D and P , the specific derivations of which are given out by Pochi Yeh and A. Mandatori et al. [19, 20]. The matrix

D depends on the directions of polarizations of four partial waves expressed by (5):

$$D(\theta) = \begin{pmatrix} \cos \theta & \cos \theta & -\sin \theta & -\sin \theta \\ n_o \cos \theta & -n_o \cos \theta & -n_e \sin \theta & n_e \sin \theta \\ \sin \theta & \sin \theta & \cos \theta & \cos \theta \\ -n_o \sin \theta & n_o \sin \theta & -n_e \cos \theta & n_e \cos \theta \end{pmatrix} \quad (5)$$

where θ is the rotation angle defined by (1).

And the matrix P is related to the phase delay quantity defined by (6):

$$P(a)$$

$$= \begin{pmatrix} \exp(-i\pi n_o a/\lambda) & 0 & 0 & 0 \\ 0 & \exp(i\pi n_o a/\lambda) & 0 & 0 \\ 0 & 0 & \exp(-i\pi n_e a/\lambda) & 0 \\ 0 & 0 & 0 & \exp(i\pi n_e a/\lambda) \end{pmatrix} \quad (6)$$

where a is the length of a single domain.

Having the duty cycle κ and the period length Λ , the total transfer matrix can be written in the form of (7):

$$M = D_a^{-1} [D(-\theta) P[\kappa(1 - \Lambda)] D^{-1} \times (-\theta) D(\theta) P(\kappa \Lambda) D(\theta)]^N D_a \quad (7)$$

where D_a is the dynamic matrix of air which is given by:

$$D_a = \begin{pmatrix} 1 & 1 & 0 & 0 \\ 1 & -1 & 0 & 0 \\ 0 & 0 & 1 & 1 \\ 0 & 0 & -1 & 1 \end{pmatrix}. \quad (8)$$

In case of normal incidence, the transmission or reflection coefficients of certain polarized incidences can be de-

rived from M . For example, the transmission of Y -direction output with the same direction input is expressed as (9)

$$T_{yy} = \left| \frac{M(1, 1)}{M(1, 1) * M(3, 3) - M(1, 3) * M(3, 1)} \right|^2. \quad (9)$$

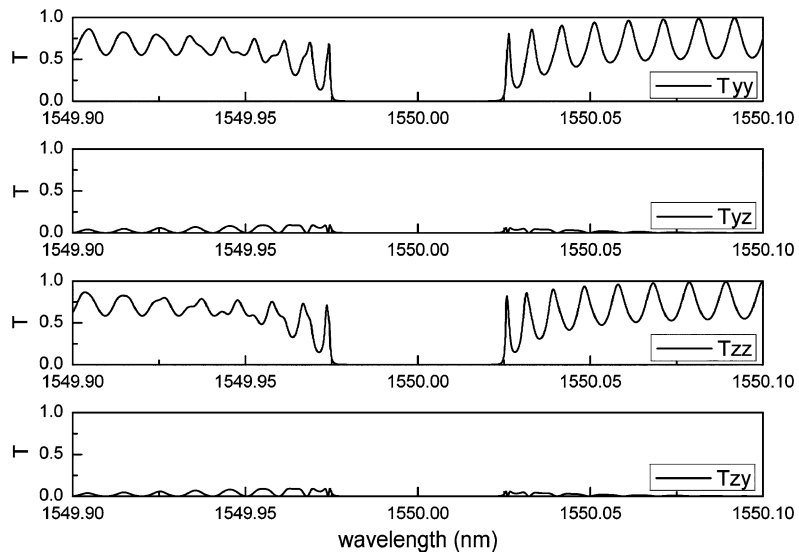
3 Simulation and discussion

In our simulations, the size of sample is set $5 \text{ cm} \times 1 \text{ cm} \times 0.5 \text{ cm}$. The poling period is satisfying the first-order ($m = 1$) Bragg condition $(n_e + n_o) \cdot \Lambda = \lambda$ for $\lambda = 1550 \text{ nm}$, which equals to 352.3 nm . The refractive index of the crystal n_e and n_o are set to 2.15 and 2.25 without electrical fields.

First of all, we consider the structure with the duty cycle $\kappa = 0.5$ and the external electrical field 300 V/mm applied along the Y axis only. Figure 2 shows the transmission spectra of light input with the Y -polarization and Z -polarization, respectively. T_{yy} and T_{zz} denote the transmission spectra where the polarizations of output fields are parallel to them of the input and T_{yz} and T_{zy} denote for the perpendicular cases. The traveling behaviors for both Y - and Z -polarized input light are quite similar at the corresponding output.

We could observe that the photonic band gaps locate in the same wavelength range at around 1550 nm with a gap width of 0.046 nm for both Y - and Z -polarized input light. The shapes of the gap in T_{yy} and T_{zz} are much deeper than in T_{yz} and T_{zy} as transmittances are over 60% at band edges. We also found that the gap width is related to the sample length, or the number of domain. If the length of sample has decreased in half (which is 2.5 cm), then to acquire the same-wide gap E_y needs to rise to 442 V/mm. The similar traveling behaviors for both Y - and Z -polarized input light, however, means that an arbitrary polarized input light could always form a gap at the same range as it can always be decomposed into Y - and Z -polarized components. Therefore,

Fig. 2 Transmission spectra of Y - and Z -polarized input and output denoted as T_{yy} T_{yz} T_{zz} T_{zy} with the electrical field of $E_y = 300 \text{ V/mm}$ applied to SPPLN, respectively



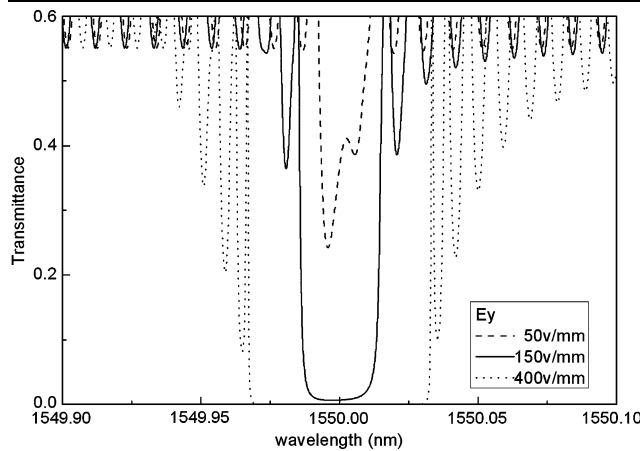


Fig. 3 Transmission spectra of Y -polarized input and output (T_{yy}) with the electrical field of $E_y = 50$ (dashed line), 150 (solid line), and 400 V/mm (dotted line) applied to SPPLN, respectively

in following discussions we only consider Y -polarized input cases for simplicity.

Figure 3 maintains the transmission spectra T_{yy} by tuning E_y . The duty cycle of the structure is set to 0.5. When E_y is set at the low level of 50 V/mm (plotted as a dashed line in Fig. 3), the forbidden gap is not deeply formed with the lowest transmittance reached around 22%. By increasing E_y to 150 V/mm (the solid line in Fig. 3), a flatly shaped gap is observed with central transmittance down to zero. When a larger E_y 400 V/mm (the dotted line in Fig. 3) is applied, the flat gap grows much wider to 0.061 nm. It shows that the depth as well as width of the gap, which is related to the mode coupling efficiency, can be modulated by E_y . Compared with other methods, such as doping or inserting new layers to gain a tunable band gap, this electrical tuning method is potentially attractive without implementing structural reconstructions.

We investigate the transmission properties when the duty cycles of structure are varying. According to the poling engineering, the most common defects that arise from the device fabrication are duty-cycle errors. Figure 4 shows the transmission spectra T_{yy} while the duty cycles are 0.5, 0.6, and 0.7, respectively and E_y is 200 V/mm. A constant duty-cycle error gives no change in gap locations other than the gap width. With duty cycle $\kappa = 0.5$, the formed gap is slightly wider than the other two; and larger deviations between positive and negative domain would lead to more suppressions of gap as shown in simulation.

Some more interesting results have been explored with duty cycle $\kappa \neq 0.5$ by applying an additional E_z . We have noticed that E_z would cause numerical deviations in n_e and n_o , thus the positive and negative domains contribute differently to the Bragg conditions due to different effective lengths. Figure 5 maintains the transmission spectra T_{yy} when an additional E_z 4000 V/mm is applied and E_y is

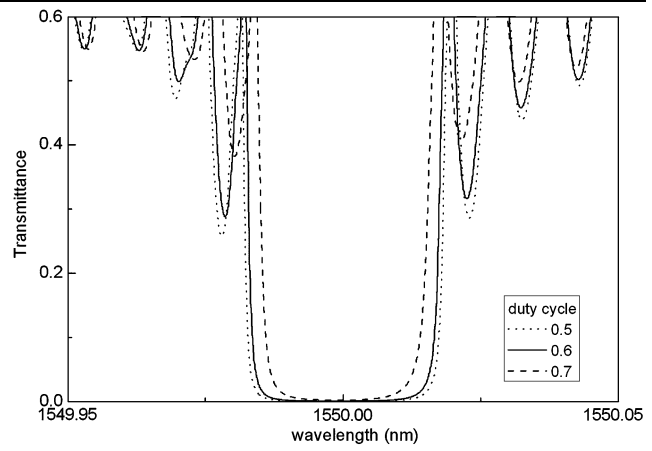


Fig. 4 Transmission spectra of Y -polarized input and output (T_{yy}) with the electrical field of $E_y = 200$ V/mm applied to SPPLN for different duty cycles 0.5, 0.6 and 0.7 in dotted, solid, and dashed lines respectively

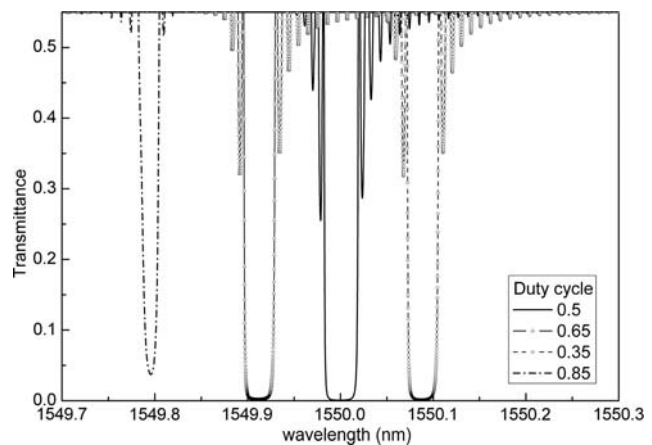


Fig. 5 Transmission spectra of Y -polarized input and output (T_{yy}) with the electrical fields of $E_y = 200$ and $E_z = 4000$ V/mm applied to SPPLN for different duty cycles 0.5, 0.65, 0.35, 0.85 in solid line, dashed line with up-triangle symbols, dashed line with circle symbols, dotted lines, and solid lines, respectively

maintained at 200 V/mm. The dashed line with up-triangle symbols, dashed line with circle symbols, dotted lines, and solid lines stand for $\kappa = 0.65$, $\kappa = 0.35$, $\kappa = 0.85$, and $\kappa = 0.5$, respectively. In the case of duty cycle $\kappa = 0.5$, the gap location remains unchanged since the induced phase variations in positive and negative domains would cancel each other according to (3). In the case of duty cycle $\kappa \neq 0.5$, however, the gap locations would be shifted as the induced phase variations in different domains are unequal. The shifted magnitude $\Delta\lambda$ which is compared to the original matched wavelength with E_y can only be expressed by E_z and duty cycle κ deduced from (4) as follows:

$$\Delta\lambda = 1.467 \times 10^{-4} \cdot (0.5 - \kappa) \cdot E_z. \quad (10)$$

According to (10), for example, the shifted magnitude $\Delta\lambda$ for $\kappa = 0.65$ is the same as $\kappa = 0.35$ but in the opposite direction. For $\kappa = 0.65$ and $E_z = 4000$ V/mm, the theoretically calculated $\Delta\lambda$ is 0.088 nm which matches well with the result in Fig. 5. Under the same E_z , $\Delta\lambda$ would shift more for greater deviations between the length of positive and negative domains, as observed for the case of $\kappa = 0.85$.

4 Conclusion

In this paper, we have investigated the electrical tunable properties of submicron periodically poled LiNbO₃(SPPLN) functioning as the forbidden band-gap structure. A narrow band gap can be acquired with a relatively low E_y . Moreover, the most efficient coupling occurs while the duty cycle is 0.5. In case of $\kappa \neq 0.5$ the gap would be shifted by additionally applying a Z-directional electrical field which is applicable in sensor devices. The electrical tuning method would also have limits, for example, the electrical field intensity could not be larger than the coercive field, otherwise deterioration of the periodical structure would result. Thus, considering the domain inversion voltage 22 kV/mm as the outer limitation, the maximum gap width could reach 1.064 nm and the dynamic range of gap location (when $\kappa = 0.6$) would be from 0 to 0.323 nm.

Since our theoretical model is supposed to be 5 cm long with 352.3-nm fabricated thin periods, some technical and practical limitations still exist. Actually, based on current studies of light induced poling effect, several groups are confident that further optimization will allow domain patterning down to length scales limited only by the diffraction limited spot size. At present, the measured domain widths of 150–300 nm are eminently compatible with structures with periods of twice this value, from 300 to 600 nm [15]. So the respective wavelength is calculated 1320 and 2640 nm for the first-order condition. Additionally, direct-write electron beam poling is promising in developing waveguide pattern structures on lithium niobate substrate which can potentially reduce the operational voltage of such devices.

Acknowledgements This research was supported by the National Natural Science Foundation of China (Nos. 60508015 and 10876006), the National Basic Research Program “973” of China (No. 2007CB-307000), the Shanghai Education Development Foundation (2007CG015), and the Shanghai Leading Academic Discipline Project (B201).

References

1. E. Yablonovitch, Inhibited spontaneous emission in solid state physics and electronics. *Phys. Rev. Lett.* **58**, 2059–2061 (1987)
2. S. John, Strong localization of photons in certain disordered dielectric superlattices. *Phys. Rev. Lett.* **58**, 2486–2488 (1987)
3. E. Yablonovitch, T.J. Gmitter, K.M. Leung, Photonic band structure: the face-centered-cubic case employing nonspherical atoms. *Phys. Rev. Lett.* **67**, 2295–2298 (1991)
4. V. Berger, Nonlinear photonic crystals. *Phys. Rev. Lett.* **81**, 4136–4139 (1998)
5. J. Armstrong, N. Bloembergen, J. Ducuing, P. Pershan, Interactions between light waves in a nonlinear dielectric. *Phys. Rev.* **127**, 1918 (1962)
6. L.E. Myers, R.C. Eckardt, M.M. Fejer, R.L. Byer, W.R. Bosenberg, J.W. Pierce, Quasi-phase-matched optical parametric oscillation in bulk periodically poled LiNbO₃. *J. Opt. Soc. Am. B* **12**, 2102–2116 (1995)
7. K. Mizuchi, K. Yamamoto, Waveguide second-harmonic generation device with broadened flat quasi-phase-matching response by use of a grating structure with located phase shifts. *Opt. Lett.* **23**, 1880–1882 (1998)
8. M. Yamada, N. Nada, M. Saitoh, K. Watanabe, First-order quasi-phase matched LiNbO₃ waveguide periodically poled by applying an external field for efficient blue second-harmonic generation. *Appl. Phys. Lett.* **62**, 435–436 (1993)
9. Y.Q. Lu, Z.L. Wan, Q. Wang, Y.X. Xi, N.B. Ming, Electro-optic effect of periodically poled optical superlattice LiNbO₃ and its applications. *Appl. Phys. Lett.* **77**, 3719–3721 (2000)
10. J.H. Shi, X.F. Chen, Y.P. Chen, Y.M. Zhu, Y.X. Xia, Y.L. Chen, Observation of solc-like filter in periodically poled lithium niobate. *Electron. Lett.* **39**, 224–225 (2003)
11. X.F. Chen, J.H. Shi, Y.P. Chen, Electro-optic solc-type wavelength filter in periodically poled lithium niobate. *Opt. Lett.* **28**, 2115–2117 (2003)
12. C. Canalias, V. Pasiskevicius, R. Clemens, F. Laurell, Submicron periodically poled flux-grown KTiOPO₄. *Appl. Phys. Lett.* **82**, 4233–4235 (2003)
13. V. Dierolf, C. Sandmann, Direct-write method for domain inversion patterns in LiNbO₃. *Appl. Phys. Lett.* **84**, 3987–3989 (2004)
14. M. Müller, E. Soergel, K. Buse, Influence of ultraviolet illumination on the poling characteristics of lithium niobate crystals. *Appl. Phys. Lett.* **83**, 1824–1826 (2003)
15. C.E. Valdivia, C.L. Sons, J.G. Scott, S. Mailis, R.W. Eason, D.A. Scrymgeour, V. Gopalan, T. Jungk, E. Soergel, I. Clark, Nanoscale surface domain formation on the +z face of lithium niobate by pulsed ultraviolet laser illumination. *Appl. Phys. Lett.* **86**, 022906 (2005)
16. C. Canalias, V. Pasiskevicius, Mirrorless optical parametric oscillator. *Nat. Photonics* **1**, 459–462 (2007)
17. N.G.R. Broderick, G.W. Ross, H.L. Offerhaus, D.J. Richardson, D.C. Hanna, Hexagonally poled lithium niobate: a two-dimensional nonlinear photonic crystal. *Phys. Rev. Lett.* **84**, 4345 (2000)
18. L. Arizmendi, Photonic applications of lithium niobate crystals. *Phys. Status Solidi A* **201**, 253–283 (2004)
19. P. Yeh, Electromagnetic propagation in birefringent layered media. *J. Opt. Soc. Am.* **69**, 742–755 (1978)
20. A. Mandatori, C. Sibilia, M. Centini, G. D’Aguanno, M. Bertolotti, M. Scalora, M. Bloemer, C.M. Bowden, Birefringence in one-dimensional finite photonic bandgap structure. *J. Opt. Soc. Am. B* **20**, 504–513 (2003)